Journal of Sound and Vibration (1997) **202**(4), 511–537

GEOMETRICAL AND SPATIAL EFFECTS ON EFFECTIVE MOBILITIES OF ANNULAR INTERFACES

B. A. T. Petersson

*Department of Aeronautical and Automotive Engineering, Loughborough University, Loughborough LE*11 3*TU, England*

(*Received* 23 *May* 1996, *and in final form* 2 *December* 1996)

An analytical and numerical study is carried out addressing the concept of interface mobilities. The introduction of such quantities would enable transmission theory to be employed for primary excitation distributions at interfaces between subsystems covering more than a fraction of the governing wavelength. Complex interface mobilities are derived for the important case of plate-like structures comprising the effective characteristics at the directly excited interface as well as transfer and cross-transfer characteristics between different interfaces. The analysis, which supplements previous work on distributed excitation [1], likewise is for annular interfaces. While the interface mobilities developed are strictly confined to such interfaces, the approach is applicable and the results are also qualitatively valid for other geometries. It is found that the direct interface mobilities can be replaced by ordinary point mobilities in the range over which the circumference (perimeter) of the interface is less than a wavelength of the governing wave. For shorter wavelengths, the interface mobilities decrease with both frequency and size of the interface. With respect to interface transfer and cross-transfer mobilities, the applicability of ordinary point quantities is, besides frequency, also dependent on the interface geometries as well as their relative, spatial locations. The mobility elements derived for the annular case are directly implementable in calculation procedures and the asymptotic expressions developed give essential information with respect to design.

1. INTRODUCTION

In a recent paper [1], a study was presented regarding the efficiency of higher order superstructure modes for the transmission of power to a connected structure being the recipient for the energy. Thereby focusing on the power transmission, the real parts of a quantity that can be termed effective "interface" mobility were indirectly addressed. It was concluded that for the frequency range of interest with respect to a class of engineering applications, only the zero and first order excitation distributions would be of concern. This class of applications comprises building structures, machine installations and built-up structural systems.

The interface problem underlying the aforementioned study is of central importance for superstructures and recipients where the contact areas between connected systems can have dimensions of the order of or larger than the governing wavelength. In reference [1] it was indicated that the applicability of transmission theory could be extended by means of introduction of effective interface mobilities. For the analysis of superstructure–recipient interaction, however, the imaginary part of the effective interface mobility is also required, and the previous study must accordingly be supplemented by results for this part. Herein, complex, effective mobilities of plate-like systems are derived and analyzed for the

0022–460X/97/190511 + 27 $25.00/0/sv960841

prominent zero and first order excitation distributions, by employing a direct Hankel transform approach. An analysis of the related problem with an axially excited cylinder, connected to a thin infinite plate in flexure, has been presented in reference [2]. In that study however, the response at a point was addressed whereas that of the complete interface is sought in the present case.

In the analysis, the interface between the two subsystems, superstructure and recipient, is assumed to be annular and continuous. In contrast to the real part of the interface mobility, this restricts the applicability of the results, since the imaginary part is sensitive to the details at the interface [3]. Accordingly, the shape of the interface will have a quantitative influence, and therefore the results are strictly valid only for an annular geometry, but reveal also important, qualitative information of the dynamic behaviour for other geometries, cf., reference [4]. Moreover, the assumed geometry facilitates the physical interpretation of the results and hence the implications of the interface effects with respect to design can be clarified. Thereby, it should also be noted that interfaces made up of groups of contact points are comprised in a qualitative sense.

In order to encompass also the more general case of multiple, large interfaces between superstructures and recipients, the response field at an adjacent interface is considered. For such cases the set of design parameters grows markedly and physically admissible simplifications are sought. Thus, in addition to the size and geometry aspects, the regions of influence as well as possible indicators for significance of the multiple interface interaction are of particular interest.

2. THEORETICAL ANALYSIS

Consider the basic superstructure–recipient configuration sketched in Figure 1. With the assumption that the superstructures are hollow, the interfaces with the recipient form two closed contour strips. Following the approach of [1], the interface is idealized to a circular contour without sacrificing generality. This means that for a thin, linearly elastic, plate-like recipient, the governing differential equation can be written as

$$L[v(r,\varphi)] + \rho''\dot{v}(r,\varphi) = \sigma(r,\varphi), \qquad \sigma(r,\varphi) = \tfrac{1}{2}\,\delta(r - R_0) \sum_{q=-\infty}^{q=\infty} \sigma_q \cos(q\varphi), \quad q \in N, \quad (1)$$

where the dot denotes differentiation with respect to time and L is the associated differential operator. A list of symbols is given in Appendix III. By employing Kirchhoff plate theory, and bearing in mind the associated limitations (cf., [3, 5]), then for harmonic excitation, the differential equation in equation (1) can be transformed into

$$\hat{v}(k)(k^4 - k_B^4) = (\mathrm{i}\omega/B')\hat{\sigma}(k). \quad (2)$$

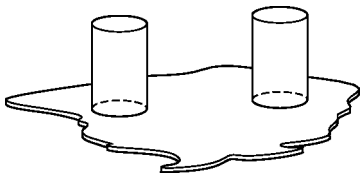

Figure 1. Two superstructures attached to plate-like recipient.

As mentioned in the introduction, two excitation distributions are of primary concern; namely, the uniform, zero order, stress

$$\sigma_F(r, \varphi) = \sigma_U \, \delta(r - R_0), \tag{3}$$

where the amplitude is obtained from the equation

$$F = \int_0^{2\pi} \int_0^{\infty} \sigma_F(r, \varphi) r \, \mathrm{d}r \, \mathrm{d}\varphi$$

and F is the net force, yielding

$$\sigma_U = F/2\pi R_0, \tag{3a}$$

and the first order "rocking" distribution

$$\sigma_M(r, \varphi) = \sigma_R \, \delta(r - R_0) \cos \varphi, \tag{4}$$

whereby the equation

$$M = \int_0^{2\pi} \int_0^{\infty} \sigma_M(r, \varphi) r^2 \cos\varphi \, \mathrm{d}r \, \mathrm{d}\varphi$$

gives the amplitude

$$\sigma_R = M/\pi R_0^2. \tag{4a}$$

By means of a Hankel transform technique, a formal solution can be straightforwardly obtained. Thereby, the wavenumber spectrum in the case of a uniform stress is found to be given by

$$\hat{\sigma}_F(k) = \int_0^{\infty} \sigma_F(r, \varphi) r \mathrm{J}_0(kr) \, \mathrm{d}r = \frac{F}{2\pi} \mathrm{J}_0(kR_0), \tag{5}$$

whereas that of the rocking distribution becomes

$$\hat{\sigma}_M(k) = \int_0^{\infty} \sigma_M(r, \varphi) r \mathrm{J}_1(kr) \, \mathrm{d}r = \frac{M}{\pi R_0} \mathrm{J}_1(kR_0) \cos \varphi. \tag{6}$$

Substituting either of the wavenumber spectra of equations (5) or (6) into equation (2) and applying an inverse transform results in the translatory velocity fields

$$v_F(r, \varphi) = \frac{\mathrm{i}\omega}{B'} \frac{F}{2\pi} \int_0^{\infty} \frac{k \mathrm{J}_0(kR_0) \mathrm{J}_0(kr) \, \mathrm{d}k}{k^4 - k_B^4} \tag{7}$$

and

$$v_M(r, \varphi) = \frac{\mathrm{i}\omega}{B'} \frac{M}{\pi R_0} \cos \varphi \int_0^{\infty} \frac{k \mathrm{J}_1(kR_0) \mathrm{J}_1(kr) \, \mathrm{d}k}{k^4 - k_B^4}, \tag{8}$$

respectively. The integrals in equations (7) and (8) are readily solved by employing the method of residues. Therefore, in the case of a zero order distribution, the integral

$$T_0 = \int_\Omega \frac{\zeta \mathrm{J}_0(\zeta a)\mathrm{J}_0(\zeta b)}{(\zeta^2 - \zeta_B^2)(\zeta^2 + \zeta_B^2)}\,\mathrm{d}\zeta \tag{9}$$

can be considered along some contour in the complex wavenumber domain. Similarly, the integral

$$T_1 = \int_\Omega \frac{\zeta \mathrm{J}_1(\zeta a)\mathrm{J}_1(\zeta b)}{(\zeta^2 - \zeta_B^2)(\zeta^2 + \zeta_B^2)}\,\mathrm{d}\zeta \tag{10}$$

is to be considered with respect to the first order distribution.

2.1. MOBILITIES AT THE EXCITED INTERFACE

The integrals T_0 and T_1 can be transcribed to all of the range $(-\infty, \infty)$ by using the identity $\mathrm{J}_n(z) = \frac{1}{2}[H_n^{(1)}(z) + \mathrm{H}_n^{(2)}(z)]$. For the region, $r \leqslant R_0$, T_0 is analytic in the upper half-plane provided that

$$T_0 = \tfrac{1}{2}\int_{-\infty}^{\infty} A(\zeta)\mathrm{J}_0(\zeta r)\mathrm{H}_0^{(1)}(\zeta R_0)\,\mathrm{d}\zeta. \tag{11}$$

As is evident from equation (9), the integrand has two real-valued poles at $\pm k_B$ and two purely imaginary ones at $\pm \mathrm{i}k_B$. Introducing a small amount of hysteretic losses shifts the location of the poles clockwise, so an integration along the real axis and along the semi-circle at infinity yields

$$T_0 = \pi\mathrm{i}\sum_{\zeta = -k_B, \mathrm{i}k_B} \mathrm{Res}\,(\zeta) = \frac{\pi\mathrm{i}R_0^2}{4}\left\{\frac{-\mathrm{J}_0(k_B r)\mathrm{J}_0(k_B R_0)}{(k_B R_0)^2} + \mathrm{i}\left[\frac{\mathrm{J}_0(k_B r)\mathrm{N}_0(k_B R_0)}{(k_B R_0)^2} + \frac{2}{\pi}\frac{\mathrm{I}_0(k_B r)\mathrm{K}_0(k_B R_0)}{(k_B R_0)^2}\right]\right\}. \tag{11a}$$

Analogously, in this spatial domain,

$$T_1 = \tfrac{1}{2}\int_{-\infty}^{\infty} A(\zeta)\mathrm{J}_1(\zeta r)\mathrm{H}_1^{(1)}(\zeta R_0)\,\mathrm{d}\zeta \tag{12}$$

is analytic in the upper half-plane and can be evaluated to give

$$T_1 = \pi\mathrm{i}\sum_{\zeta = -k_B, \mathrm{i}k_B} \mathrm{Res}\,(\zeta) = \frac{\pi\mathrm{i}R_0^2}{4}\left\{\frac{-\mathrm{J}_1(k_B r)\mathrm{J}_1(k_B R_0)}{(k_B R_0)^2} + \mathrm{i}\left[\frac{\mathrm{J}_1(k_B r)\mathrm{N}_1(k_B R_0)}{(k_B R_0)^2} + \frac{2}{\pi}\frac{\mathrm{I}_1(k_B r)\mathrm{K}_1(k_B R_0)}{(k_B R_0)^2}\right]\right\}. \tag{12a}$$

Owing to the fact that the symmetric and anti-symmetric excitation distributions are treated separately, it is relevant to consider a spatially averaged response, formed on a

complex power basis, in developing the mobility [6]. Thus, the two interface mobility components are obtained from

$$\overline{Y_{vF}} = \frac{\int_0^{2\pi}\int_0^{\infty} v_F(r,\varphi)\sigma_F^*(r,\varphi)r\,\mathrm{d}r\,\mathrm{d}\varphi}{\left|\int_0^{2\pi}\int_0^{\infty}\sigma_F(r,\varphi)r\,\mathrm{d}r\,\mathrm{d}\varphi\right|^2} \tag{13}$$

and

$$\overline{Y_{wM}} = \frac{\int_0^{2\pi}\int_0^{\infty} v_F(r,\varphi)\sigma_M^*(r,\varphi)r\,\mathrm{d}r\,\mathrm{d}\varphi}{\left|\int_0^{2\pi}\cos\sigma\int_0^{\infty}\sigma_M(r,\varphi)r^2\,\mathrm{d}r\,\mathrm{d}\varphi\right|^2}, \tag{14}$$

respectively. The implicit symmetry of an infinite system means that the cross-mobilities at the excited interface from force to rotational velocity as well as from moment to translatory velocity vanish identically. Substituting the appropriate ingredients into equations (13) and (14) leads to

$$\overline{Y_{vF}} = \frac{\omega}{B'}\frac{R_0^2}{8}\left\{\left[\frac{\mathrm{J}_0(k_BR_0)}{(k_BR_0)}\right]^2 - \mathrm{i}\left[\frac{\mathrm{J}_0(k_BR_0)\mathrm{N}_0(k_BR_0)}{(k_BR_0)^2} + \frac{2}{\pi}\frac{\mathrm{I}_0(k_BR_0)\mathrm{K}_0(k_BR_0)}{(k_BR_0)^2}\right]\right\} \tag{13a}$$

and

$$\overline{Y_{wM}} = \frac{\omega}{4B'}\left\{\left[\frac{\mathrm{J}_1(k_BR_0)}{(k_BR_0)}\right]^2 - \mathrm{i}\left[\frac{\mathrm{J}_1(k_BR_0)\mathrm{N}_1(k_BR_0)}{(k_BR_0)^2} - \frac{2}{\pi}\frac{\mathrm{I}_1(k_BR_0)\mathrm{K}_1(k_BR_0)}{(k_BR_0)^2}\right]\right\} \tag{14a}$$

for the two principal excitation distributions.

As the Helmholtz number becomes small, the asymptotes for the real and imaginary parts of the mobilities can be developed as

$$\mathrm{Re}\,[\overline{Y_{vF}}] \to \frac{\omega}{8B'k_B^2}, \qquad \mathrm{Im}\,[\overline{Y_{vF}}] \to \frac{\omega}{8B'k_B^2}\frac{2\mathrm{i}}{\pi}(k_BR_0)^2[\ln(k_BR_0/2) + \gamma_E - \tfrac{1}{2}] \tag{15a, b}$$

in the case of a uniform distribution. Hereby, it is seen that while the real part, as expected, approaches that of a point excited, thin infinite plate, the imaginary part does not vanish identically but reveals an anomaly in the sense that the spatially averaged reactivity is that of a "negative spring". Indeed, this imaginary part is small, and vanishes as the Helmholtz number goes to zero but, nonetheless, a spring-like behaviour is not encountered below a Helmholtz number of unity in the ordinary point excitation case. For the annular interface, the enclosed area is responding oppositely to that of the exterior domain which affects the integrated reactivity.

For the moment mobility, the corresponding trends are found to be given by

$$\mathrm{Re}\,[\overline{Y_{wM}}] \to \frac{\omega}{16B'}, \qquad \mathrm{Im}\,[\overline{Y_{wM}}] \to \frac{\omega}{16B'}\frac{4\mathrm{i}}{\pi}[\ln(2/k_BR_0) - \gamma_E + \tfrac{1}{4}], \tag{16a, b}$$

both of which conform to the behaviour of the point moment excited plate, although the constant term within brackets of the imaginary part depends on the actual excitation condition.

In the opposite instance, in which the Helmholtz number grows large, the trend of the force mobility is described by

$$\overline{Y_{vF}} = \frac{\omega}{8B'k_B^2}\frac{1}{\pi k_B R_0}\{1 + \sin 2k_B R_0 - \mathrm{i}[1 - \cos 2k_B R_0]\}, \tag{15c}$$

and it is seen that the characteristics resemble those of the infinite beam with an overall, mass controlled imaginary part. Also, for the moment mobility,

$$\overline{Y_{wM}} = \frac{\omega}{16B'}\frac{4}{\pi(k_B R_0)^3}\{1 - \sin 2k_B R_0 + \mathrm{i}[1 - \cos 2k_B R_0]\}, \tag{16c}$$

the beam-like signature is established with the stiffness controlled imaginary part. It should be emphasized that all expressions discussed above concern the mobility with respect to the directly excited, annular interface.

2.2. TRANSFER AND CROSS-TRANSFER MOBILITIES

For the spatial domain in which $r > R_0$, the integrals to consider are

$$T_{0r} = \tfrac{1}{2}\int_{-\infty}^{\infty} A(\zeta)\mathrm{J}_0(\zeta R_0)\mathrm{H}_0^{(1)}(\zeta r)\,\mathrm{d}\zeta \quad \text{and} \quad T_{1r} = \tfrac{1}{2}\int_{-\infty}^{\infty} A(\zeta)\mathrm{J}_1(\zeta R_0)\mathrm{H}_1^{(1)}(\zeta r)\,\mathrm{d}\zeta, \tag{17, 18}$$

for the two distributions respectively. In this case, the method of residues yields

$$T_{0r} = \pi\mathrm{i}\sum_{\zeta = -k_B, \mathrm{i}k_B}\mathrm{Res}\,(\zeta) = \frac{\pi\mathrm{i}R_0^2}{4}\left\{-\frac{\mathrm{J}_0(k_B R_0)\mathrm{J}_0(k_B r)}{(k_B R_0)^2}\right.$$

$$\left. + \mathrm{i}\left[\frac{\mathrm{J}_0(k_B R_0)\mathrm{N}_0(k_B r)}{(k_B R_0)^2} + \frac{2}{\pi}\frac{\mathrm{I}_0(k_B R_0)\mathrm{K}_0(k_B r)}{(k_B R_0)^2}\right]\right\} \tag{17a}$$

and

$$T_{1r} = \pi\mathrm{i}\sum_{\zeta = -k_B, \mathrm{i}k_B}\mathrm{Res}\,(\zeta) = \frac{\pi\mathrm{i}R_0^2}{4}\left\{-\frac{\mathrm{J}_1(k_B R_0)\mathrm{J}_1(k_B R_0 r)}{(k_B R_0)^2}\right.$$

$$\left. + \mathrm{i}\left[\frac{\mathrm{J}_1(k_B R_0)\mathrm{N}_1(k_B r)}{(k_B R_0)^2} + \frac{2}{\pi}\frac{\mathrm{I}_1(k_B R_0)\mathrm{K}_1(k_B r)}{(k_B R_0)^2}\right]\right\} \tag{18a}$$

This means that the translatory responses are obtained as

$$v_F(r) = \frac{\omega}{8B'k_B^2}F_0\left\{\mathrm{J}_0(k_B R_0)\mathrm{J}_0(k_B r) - \mathrm{i}\left[\mathrm{J}_0(k_B R_0)\mathrm{N}_0(k_B r) + \frac{2}{\pi}\mathrm{I}_0(k_B R_0)\mathrm{K}_0(k_B r)\right]\right\} \tag{19}$$

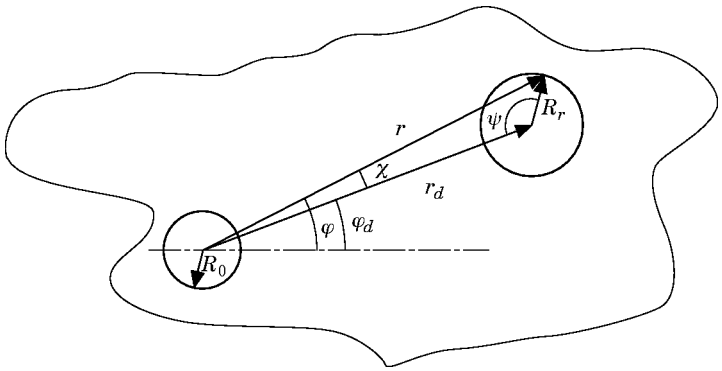

Figure 2. Annular source and receiver interfaces with the adopted notation.

and

$$v_M(r, \varphi) = \frac{\omega}{4B'k_B}\frac{M_0}{(k_BR_0)}\cos\varphi\Bigg\{\mathrm{J}_1(k_BR_0)\mathrm{J}_1(k_Br) - \mathrm{i}\Bigg[\mathrm{J}_1(k_BR_0)\mathrm{N}_1(k_Br) + \frac{2}{\pi}\mathrm{I}_1(k_Br_0)\mathrm{K}_1(k_Br)\Bigg]\Bigg\}. \tag{20}$$

The rotational responses are readily obtained from the gradient of the translational velocity which, projected on to the component directions, can be written as

$$w_M(r, \varphi) = \frac{\omega}{4B'}\frac{M_0}{(k_BR_0)}\Bigg((\cos\varphi, -\sin\varphi)\cos\varphi\Bigg\{\mathrm{J}_1(k_BR_0)\Bigg(\mathrm{J}_0(k_Br) - \frac{1}{k_Br}\mathrm{J}_1(k_Br)\Bigg) - \mathrm{i}\Bigg[\mathrm{J}_1(k_BR_0)\Bigg(\mathrm{N}_0(k_Br) - \frac{1}{k_Br}\mathrm{N}_1(k_Br)\Bigg) - \frac{2}{\pi}\mathrm{I}_1(k_BR_0) \times \Bigg(\mathrm{K}_0(k_Br) + \frac{1}{k_Br}\mathrm{K}_1(k_Br)\Bigg)\Bigg]\Bigg\} + (\sin\varphi, \cos\varphi)\frac{\sin\varphi}{k_Br}\Bigg\{\mathrm{J}_1(k_BR_0)\mathrm{J}_1(k_Br) - \mathrm{i}\Bigg[\mathrm{J}_1(k_BR_0)\mathrm{N}_1(k_Br) + \frac{2}{\pi}\mathrm{I}_1(k_BR_0)\mathrm{K}_1(k_Br)\Bigg]\Bigg\}\Bigg). \tag{21}$$

For small Helmholtz numbers, now based on the size of the response interface, the spatial averaging is irrelevant, since the governing wavelength is large and the transfer mobilities follow from equations (19) and (21). As the Helmholtz number approaches unity and above, the variation over the response interface can become significant and must be taken into account. Although the precise treatment will differ slightly for various interface geometries, it is again appropriate to consider an annular interface as outlined in Figure 2.

From the law of the cosine,

$$r = \sqrt{r_d^2 + R_r^2 - 2r_d R_r \cos\psi}, \tag{22}$$

with equation (19), the pure force transfer mobility becomes

$$\overline{Y_{vF}}(r_d) = \frac{\omega}{8B'k_B^2}\frac{1}{2\pi}\int_0^{2\pi}\left\{\mathrm{J}_0(k_BR_0)\mathrm{J}_0(k_Br) - \mathrm{i}\left[\mathrm{J}_0(k_BR_0)\mathrm{N}_0(k_Br) + \frac{2}{\pi}\,\mathrm{J}_0(k_BR_0)\mathrm{K}_0(k_Br)\right]\right\}\mathrm{d}\psi, \tag{23}$$

while those due to a moment, assumed acting along $\varphi = \pi/2$, would be obtained from averaging

$$\begin{aligned} Y_{wM,\parallel}(r,\varphi) = \frac{\omega}{4B'}\frac{1}{(k_BR_0)}\Bigg\{\cos^2\varphi\Bigg\{\mathrm{J}_1(k_BR_0)\left[\mathrm{J}_0(k_Br) - \frac{1}{k_Br}\,\mathrm{J}_1(k_Br)\right] \\ - \mathrm{i}\left[\mathrm{J}_1(k_BR_0)\left[\mathrm{N}_0(k_Br) - \frac{1}{k_Br}\,\mathrm{N}_1(k_Br)\right] - \frac{2}{\pi}\,\mathrm{I}_1(k_BR_0)\right. \\ \left.\times\left[\mathrm{K}_0(k_Br) + \frac{1}{k_Br}\,\mathrm{K}_1(k_Br)\right]\right]\Bigg\} + \frac{\sin^2\varphi}{k_Br}\Bigg\{\mathrm{J}_1(k_BR_0)\mathrm{J}_1(k_Br) \\ - \mathrm{i}\left[\mathrm{J}_1(k_BR_0)\mathrm{N}_1(k_Br) + \frac{2}{\pi}\,\mathrm{I}_1(k_BR_0)\mathrm{K}_1(k_Br)\right]\Bigg\}\Bigg) \\ = \frac{\omega}{8B'}\frac{1}{(k_BR_0)}\left(\left[\mathrm{J}_1(k_BR_0)\mathrm{H}_0^{(2)}(k_Br) + \mathrm{i}\,\frac{2}{\pi}\,\mathrm{I}_1(k_BR_0)\mathrm{K}_0(k_Br)\right]\right. \\ \left. - \cos 2\varphi\left[\mathrm{J}_1(k_BR_0)\mathrm{H}_2^{(2)}(k_Br) - \mathrm{i}\,\frac{2}{\pi}\,\mathrm{I}_1(k_BR_0)\mathrm{K}_2(k_Br)\right]\right) \end{aligned} \tag{24a}$$

and

$$Y_{wM,\perp}(r,\varphi) = \frac{\omega}{8B'}\frac{\sin 2\varphi}{(k_BR_0)}\left\{\mathrm{J}_1(k_BR_0)\mathrm{H}_2^{(2)}(k_Br) - \mathrm{i}\,\frac{2}{\pi}\,\mathrm{I}_1(k_BR_0)\mathrm{K}_2(k_Br)\right\}. \tag{24b}$$

Here, the indices $\perp$ and $\parallel$ denote that the rotational velocity vector is perpendicular to or in parallel with that of the moment.

For the integral in equation (23) one can, after some manipulation (see Appendix I), find that spatial averaging gives

$$\overline{Y_{vF}}(r_d) = \frac{\omega}{8B'k_B^2}\left\{\mathrm{J}_0(k_BR_0)\mathrm{J}_0(k_BR_r)[\mathrm{J}_0(k_Br_d) - \mathrm{i}\mathrm{N}_0(k_Br_d)]\right.$$

$$\left. - \mathrm{i}\frac{2}{\pi}\,\mathrm{I}_0(k_BR_0)\mathrm{I}_0(k_BR_r)\mathrm{K}_0(k_Br_d)\right\}. \quad (25)$$

As one would expect, the force mobility is symmetric with respect to excitation and response interfaces and the nearfield term is important only for interfaces close to each other. Also, it is clear that the force transfer mobility in equation (25) degenerates to that of a response at r_d for small enough k_BR_r.

Moreover, for low frequencies, one finds an asymptotic behaviour described by

$$\mathrm{Re}[\overline{Y_{vF}}(r_d)] \to \frac{\omega}{8B'k_B^2}\left\{1 - \tfrac{1}{4}[(k_BR_0)^2 + (k_BR_r)^2 + (k_Br_d)^2]\right\} \quad (26a)$$

and

$$\mathrm{Im}[\overline{Y_{vF}}(r_d)] \to \frac{\omega}{8B'k_B^2}\frac{(k_Br_d)^2}{\pi}\left[\ln\left(\frac{k_Br_d}{2}\right) + \gamma_E + 1\right] \quad (26b)$$

for the real and imaginary parts respectively. It is seen that while the real part depends on both geometry and separation, the imaginary part is influenced only by the latter.

Unfortunately, the integrals involving equations (24) are not equally amenable to analytic treatment. An alternative approach to assess the moment to rotational velocity interface transfer mobility (effective) is to derive the first order Fourier component of the

TABLE 1

Definition of interface mobility elements

Direct interface mobility	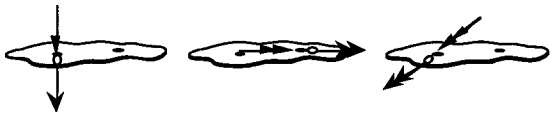
Interface transfer mobility	
Interface cross-transfer mobility	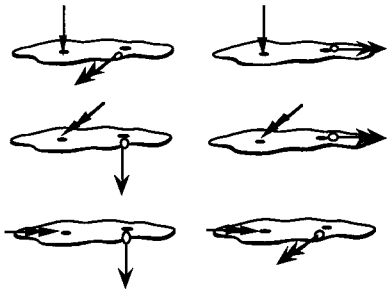

translatory velocity from equation (20) and subsequently project this on to the co-linear and perpendicular set of main axes, see Table 1. In such a case, the moment transfer mobility can be formally written as

$$\frac{w_M(r_d, \varphi_d)}{M_0 R_r} = -\frac{\omega}{4B' k_B R_r} \frac{1}{(k_B R_0)} \frac{1}{\pi} \int_{-\pi}^{\pi} (\cos(\psi - \varphi_d), \sin(\psi - \varphi_d)) \cos(\varphi_d + \chi),$$

$$\times \left\{ J_1(k_B R_0) H_1^{(2)}(k_B r) - i \frac{2}{\pi} I_1(k_B R_0) K_1(k_B r) \right\} d\psi, \tag{27}$$

which, in view of Graf's addition theorem, leads to (see Appendix II)

$$\overline{Y_{wM,\parallel}}(r_d, \varphi_d) = \frac{\omega}{4B'} \left\{ \frac{J_1(k_B R_0)}{(k_B R_0)} \frac{J_1(k_B R_r)}{(k_B R_r)} [H_0^{(2)}(k_B r_d) - \cos 2\varphi_d H_2^{(2)}(k_B r_d)] \right.$$

$$\left. + i \frac{2}{\pi} \frac{I_1(k_B R_0)}{(k_B R_0)} \frac{I_1(k_B R_r)}{(k_B R_r)} [K_0(k_B r_d) + \cos 2\varphi_d K_2(k_B r_d)] \right\} \tag{28a}$$

and

$$\overline{Y_{wM,\perp}}(r_d, \varphi_d) = \frac{\omega}{4B'} \sin 2\varphi_d \left\{ \frac{J_1(k_B R_0)}{(k_B R_0)} \frac{J_1(k_B R_r)}{(k_B R_r)} [H_2^{(2)}(k_B r_d)] \right.$$

$$\left. - i \frac{2}{\pi} \frac{I_1(k_B R_0)}{(k_B R_0)} \frac{I_1(k_B R_r)}{(k_B R_r)} K_2(k_B r_d) \right\} \tag{28b}$$

for the two mobility elements respectively. A comparison of equations (24) and (28) reveals that they agree for small enough $k_B R_r$. As for the force transfer mobility, reciprocity is seen in the spatially averaged results. For large wavenumbers it is observed that the dependence on the interface geometry essentially is that of a $(\sin z)/z$ divided by the geometrical mean of the two Helmholtz numbers for the excitation and response interfaces. It can thus be inferred that the moment transfer mobilities decrease with an increase in frequency, size of interface and distance, wherefore it is reasonable to focus on the range of Helmholtz numbers below unity. In this range the asymptotic behaviour of the real parts are essentially governed by the point characteristics, so that

$$\mathrm{Re}\,[\overline{Y_{wM,\parallel}}(r_d, \varphi_d)] \to \frac{\omega}{16B'} \left\{ 1 - \frac{(k_B r_d)^2}{4} \left[1 - \frac{\cos 2\varphi_d}{2} \right] \right\} \tag{29a}$$

and

$$\mathrm{Re}\,[\overline{Y_{wM,\perp}}(r_d, \varphi_d)] \to \frac{\omega}{16B'} \sin 2\varphi_d \frac{(k_B r_d)^2}{8}, \tag{30a}$$

while those of the imaginary parts are somewhat more involved and are found to be given by

$$\mathrm{Im}\,[\overline{Y_{wM,\parallel}}(r_d, \varphi_d)] \to \frac{\omega}{16B'} \left\{ \frac{4}{\pi} \left[\ln\left(\frac{2}{k_B r_d}\right) - \gamma_E \right] - \frac{\cos 2\varphi_d}{\pi} \left[2 - \left(\frac{R_0}{r_d}\right)^2 - \left(\frac{R_r}{r_d}\right)^2 \right] \right\} \tag{29b}$$

and

$$\mathrm{Im}\,[\overline{Y_{wM,\perp}}(r_d,\varphi_d)] \to \frac{\omega}{16B'}\frac{\sin 2\varphi_d}{\pi}\left\{2-\left(\frac{R_0}{r_d}\right)^2-\left(\frac{R_r}{r_d}\right)^2\right\}, \tag{30b}$$

respectively. From the asymptotic expressions it is observed that the imaginary parts of the moment mobilities depend on the ratios of the typical size of the interface to the separation distance and the angle. It must be emphasized that neither of these ratios can exceed unity in practice. It is also interesting to note that no peculiarities are introduced in the limiting case, as the radii of either interface tend to zero for a moment mobility element derived in this manner. For the pure moment transfer mobility element, a decrease in the reactive part is obtained for decreasing ratios when the angle is small, whereas the reactive part increases for large angles. With respect to the moment cross-transfer element, a decrease of the ratios consistently leads to an increase in the reactive part. A similar geometry dependence does not exist for the force transfer mobility. This means that there is an interesting configuration feature implied by the moment mobilities in that, for those cases in which a predominant vectorial moment component can be identified, the orientation of superstructures situated side-by-side, along a line perpendicular to the moment vector, should preferably be designed to be long in the direction of the moment. This conclusion also holds for a lateral force excitation at the top of a superstructure, resulting in a corresponding moment excitation of the recipient. Moreover, superstructures, adjacent in the direction of the moment, should be closely spaced. Accordingly, it appears reasonable to "extrapolate" these conclusions into two parallel, narrow superstructures, co-linear with the predominant moment but well spaced in the orthogonal direction, as an advantageous configuration for small Helmholtz numbers in order to reduce the influence of the transfer path via a plate-like recipient.

Finally, the interface cross-transfer mobility from moment to translatory velocity or, reciprocally, from force to rotational velocity, can be derived in a completely analogous manner by considering equation (20). Thus, a spatial averaging over the (annular) response interface yields

$$\begin{aligned}\overline{Y_{vM}}(r_d,\varphi_d) &= \frac{\omega}{4B'k_B}\frac{1}{(k_BR_0)}\frac{1}{2\pi}\int_{-\pi}^{\pi}\cos(\varphi_d+\chi)\Big\{\mathrm{J}_1(k_BR_0)\mathrm{J}_1(k_Br)\\ &\quad -\mathrm{i}\Big[\mathrm{J}_1(k_BR_0)\mathrm{N}_1(k_Br)+\frac{2}{\pi}\mathrm{I}_1(k_BR_0)\mathrm{K}_1(k_Br)\Big]\Big\}\,\mathrm{d}\psi\\ &= \frac{\omega}{4B'k_B}\cos\varphi_d\Big\{\frac{\mathrm{J}_1(k_BR_0)}{(k_BR_0)}\mathrm{J}_0(k_BR_r)\mathrm{H}_1^{(2)}(k_Br_d)\\ &\quad -\mathrm{i}\frac{2}{\pi}\frac{\mathrm{I}_1(k_BR_0)}{(k_BR_0)}\mathrm{I}_0(k_BR_r)\mathrm{K}_1(k_Br_d)\Big\}.\end{aligned} \tag{31}$$

It is seen that the propagation function is anti-symmetric, so that the mobility is no longer symmetric with respect to the excitation and response interfaces. This means that in order to obtain the force to rotational velocity cross-transfer component, the indices R_0 and R_r

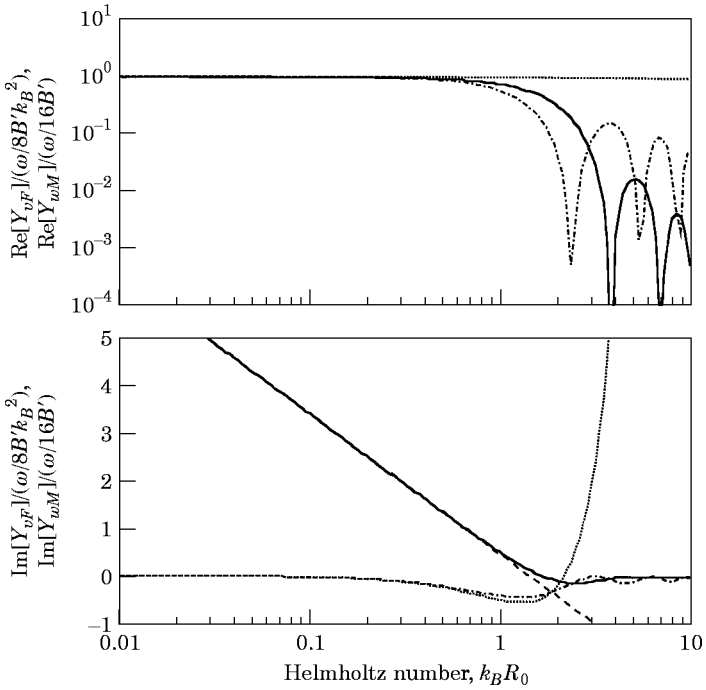

Figure 3. Normalized real (top) and imaginary (bottom) parts of moment (——) and force (–·–·–) mobility. Asymptotic behaviour of moment (---) and force (····) mobilities for small Helmholtz numbers.

must be interchanged in equation (31). For low frequencies and small dimensions of the two interfaces the asymptotic behaviour

$$\mathrm{Re}\,[\overline{Y_{vM}}(r_d, \varphi_d)] \to \frac{\omega}{4B'k_B}\cos\varphi_d\frac{k_Br_d}{4}\left\{1-\frac{(k_BR_0)^2}{8}-\frac{(k_BR_r)^2}{4}\right\}, \tag{32a}$$

$$\mathrm{Im}\,[\overline{Y_{vM}}(r_d, \varphi_d)] \to -\frac{\omega}{4B'k_B}\cos\varphi_d\frac{k_Br_d}{\pi}\left\{\ln\left(\frac{k_Br_d}{2}\right)+\gamma_E-\tfrac{1}{2}+\tfrac{1}{4}\left(\frac{R_0}{r_d}\right)^2+\tfrac{1}{2}\left(\frac{R_r}{r_d}\right)^2\right\} \tag{32b}$$

clearly illuminate the non-symmetry. Roughly, this cross-transfer mobility element initially grows linearly with frequency and distance between the two interfaces. The imaginary part is additionally influenced by a logarithmic dependence on frequency and distance. The asymptotes also show that the size and orientation of the interfaces play a role. Moreover, from the last part of equation (31) it is noted that, for large arguments, the mobility will decrease, and hence it can be deduced that a maximum occurs in the transition region from "near" to "farfield" behaviour.

3. NUMERICAL ANALYSIS

In Figure 3 are shown the direct moment and force effective mobilities for an annular interface, normalized with respect to the real parts of the corresponding ordinary point mobilities. Also included are the asymptotes for small Helmholtz numbers according to equations (15) and (16). It is seen that the annular interface has a negligible effect on force as well as moment mobility, relative to that of ordinary point excitation, as long as the

circumference is less than the governing wavelength or, equivalently, the radius is less than a sixth of the wavelength. In this range, the asymptotes derived can be regarded as virtually exact. As frequency or the radius increases, the mobility diminishes and exhibits rounded maxima and pronounced minima, a feature that has been discussed in more detail in reference [1]. Apart from the region in the immediate vicinity of $k_B R_0$ equals unity, also the asymptotes according to equations (15c) and (16c) operate satisfactorily. It is worth noting that in the upper range, the real parts of moment and force mobilities have envelopes with identical frequency dependencies in an absolute sense and the discrepancy established in the diagram is a result of different normalizations. As anticipated, the reactive parts oscillate around zero, and for Helmholtz numbers above unity settle down having envelopes identical to those of the real parts. In contrast, the signatures for small Helmholtz numbers are different and conform to those of the point quantities. For the imaginary parts, the weakly negative force mobility and the weakly "hardening" stiffness controlled moment mobility can be observed.

It is thus clear that ordinary point mobilities are applicable with negligible loss in accuracy in the range of Helmholtz numbers below unity but that above there the concept of interface mobility should be employed. Particular attention must be paid to the region around unity whereas, for higher frequencies and large interfaces, the asymptotic expressions yield valid results. From a design point of view, however, the information furnished by the asymptotic relations is appropriate.

In Figure 4, the interface force transfer mobility is presented. For consistency, all transfer and cross-transfer mobilities are displayed versus the same Helmholtz number, $k_B R_0$, as the direct interface mobilities. This is, however, not always the most appropriate choice for the interpretation owing to the fact that for some transfer mobilities, the distance between the excitation and response interfaces turns out to be more influential than the typical size of the interface. Accordingly, the region of applicability of the associated asymptotic expressions are more conveniently assessed from a Helmholtz number equal

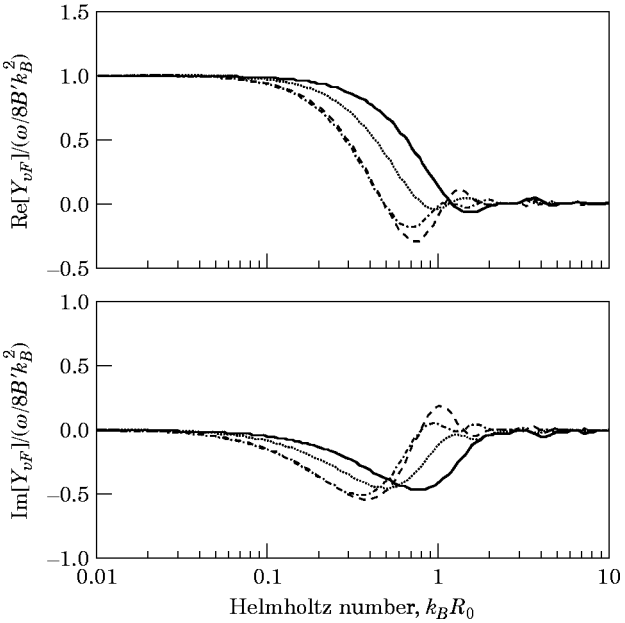

Figure 4. Normalized real (top) and imaginary (bottom) parts of force transfer mobility. $R_r/R_0 = 1$, $R_d/r_0 = 2$; (——), $R_r/R_0 = 1$; $r_d/R_0 = 5$; (— —), $R_r/R_0 = 2$; $r_d/R_0 = 3$; (·····), $R_r/R_0 = 2$; $r_d/R_0 = 5$; (–·–·–).

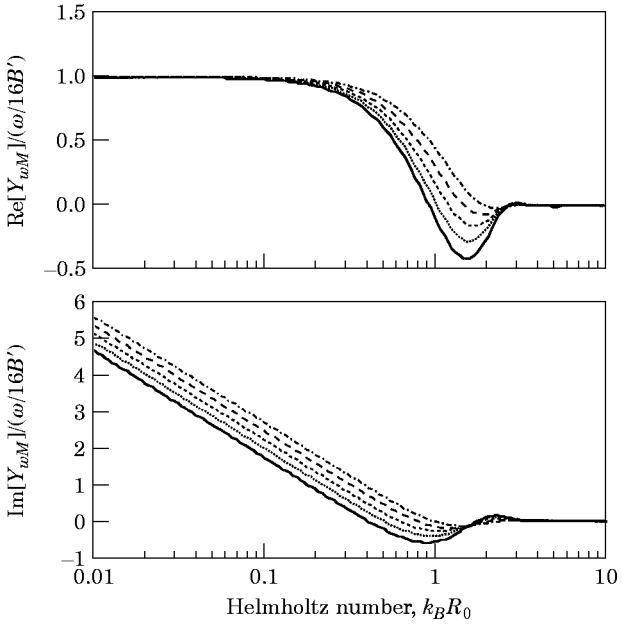

Figure 5. Normalized real (top) and imaginary (bottom) parts of moment transfer mobility. $R_r/R_0 = 1$, $r_d/R_0 = 2$. ——, $\varphi_d = 0$; ·····, $\varphi_d = \pi/6$; - - - -, $\varphi_d = \pi/4$; — —, $\varphi_d = \pi/3$; –·–·–, $\varphi_d = \pi/2$.

to unity when based on the distance r_d. This limit also constitutes the important transition from a "nearfield" to a "farfield" behaviour.

It is observed in Figure 4 that the "nearfield" behaviour is featured by that of the associated ordinary point mobility. Above there, a marked transition region is obtained in which all geometrical parameters are influential. Finally, the "farfield" behaviour is seen to render comparatively small contributions from one interface to the other. As for the direct interface mobilities, particular attention should be paid the transition region.

The qualitative trend and geometrical parameter influence are those described by the asymptotic expressions given in equations (26). Furthermore, it is found from the numerical results that the interface geometry is influential mainly in the range below a Helmholtz number of unity, a finding which is important with respect to both prediction and design. Accordingly, the effects of the reactive parts cannot be neglected for multiple interfaces subject to force excitation.

The interface moment transfer mobility is shown in Figures 5–8 for some ratios of interface dimensions and separations. Owing to the additional angular dependence, the influence of interface separation and size is presented in four diagrams. For adjacent interfaces of similar dimensions, illustrated in Figure 5, it is demonstrated that the angular dependence is mainly confined to the transition region regarding the real part while the angle affects all of the "nearfield" behaviour of the imaginary part. When the dimension of either interface is enlarged, the angular dependence is only minutely diminished, which is established from a comparison of Figures 5 and 6. In contrast, the effect is more pronounced when the interface separation is increased but still essentially confined to the transition and nearfield regions respectively; see Figure 7. As could be expected from a wave-theoretical point of view, the real and imaginary parts exhibit oscillatory signatures for large Helmholtz numbers, which is clearly manifested as the distance from the excitation to the response interface increases. The transition from "nearfield" to "farfield" behaviour is shifted to smaller Helmholtz numbers, resulting in a small decrease in the

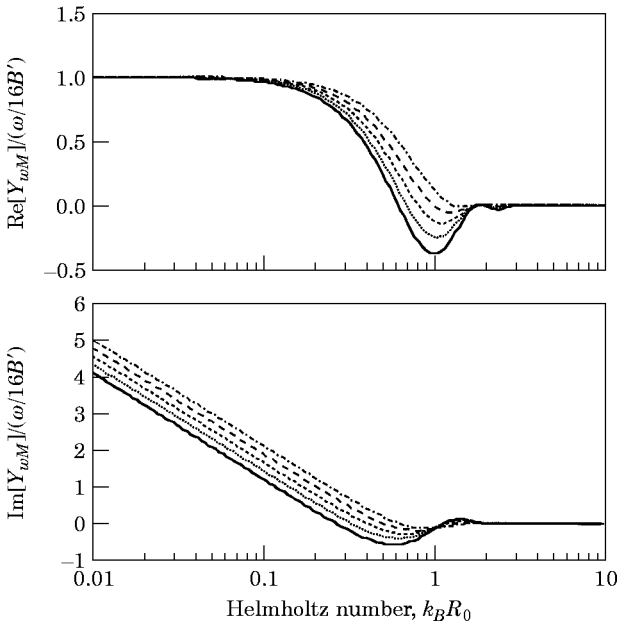

Figure 6. Normalized real (top) and imaginary (bottom) parts of moment transfer mobility. $R_r/R_0 = 2$, $r_d/R_0 = 3$. ——, $\varphi_d = 0$; ·····, $\varphi_d = \pi/6$; - - - -, $\varphi_d = \pi/4$; — —, $\varphi_d = \pi/3$; –·–·–, $\varphi_d = \pi/2$.

mobilities. In this example one may observe the wave effect which is superimposed on the angular dependence. This means that as the phase relation is reversed between the excitation and response interfaces, and so is the angular dependence. Accordingly, the analytical findings discussed in conjunction with equations (28a) and (29a) are relevant

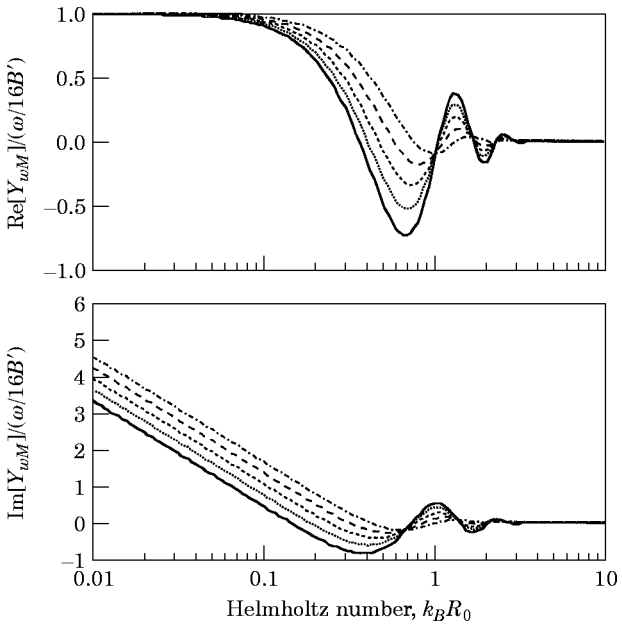

Figure 7. Normalized real (top) and imaginary (bottom) parts of moment transfer mobility. $R_r/R_0 = 1$, $r_d/R_0 = 5$. ——, $\varphi_d = 0$; ·····, $\varphi_d = \pi/6$; - - - - , $\varphi_d = \pi/4$; — —, $\varphi_d = \pi/3$; –·–·–, $\varphi_d = \pi/2$.

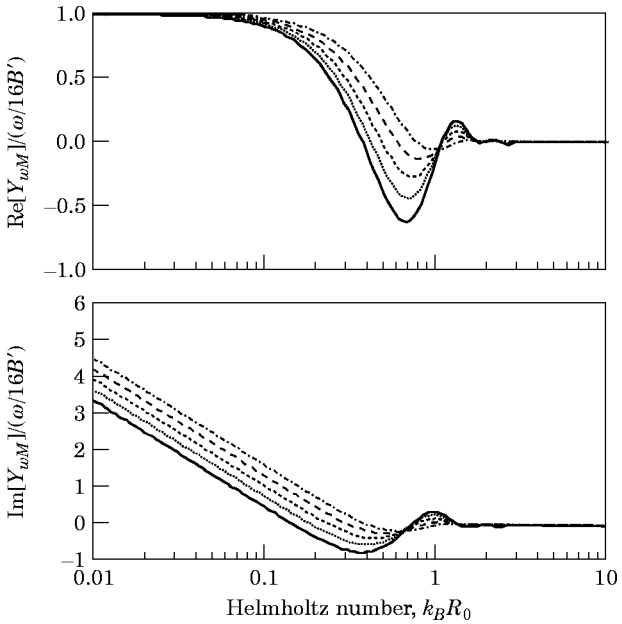

Figure 8. Normalized real (top) and imaginary (bottom) parts of moment transfer mobility. $R_r/R_0 = 2$, $r_d/R_0 = 5$. ——, $\varphi_d = 0$; ·····, $\varphi_d = \pi/6$; - - - -, $\varphi_d = \pi/4$; — —, $\varphi_d = \pi/3$; –·–·–, $\varphi_d = \pi/2$.

only for the "nearfield" behaviour. An increase in the ratio of the typical dimensions of response to those of the excitation interfaces has a negligible effect on the mobilities for small Helmholtz numbers whereas the "farfield" behaviour is smoothed; compare Figures 7 and 8. It is thus generally beneficial for designs, operating at high frequencies, to utilize differing and comparatively large size cross-sections.

The features of the interface moment cross-transfer mobility are displayed in Figures 9–12. As for the transfer mobility, the parameter is the angle between the excitation and response interfaces, relative to an axis perpendicular to the moment vector, see Figure 2. It is clearly established that the real part is most significant in the transition region and has a maximum for an angle of 45°. The imaginary part, on the other hand, is large and stiffness controlled in the region of "nearfield" behaviour. Moreover, and in agreement with the transfer mobility, an enlargement of either the excitation or response interface results in a minute reduction of the mobility for small Helmholtz numbers, compare Figures 9 and 10 as well as Figures 11 and 12.

The influence of the separation between the two interfaces, in contrast, is more pronounced as can be seen from a comparison of Figures 9 and 11 or Figures 10 and 12, where also the phase progress is clearly established. An increase in the separation affects the moment cross-transfer mobility in two ways. First, the maxima of both parts increase, the real being governed by the second order Bessel function and the imaginary approach $2/\pi$ when normalized; cf., equations (28b) and (30b) respectively. Second, the maxima are shifted towards smaller Helmholtz numbers. This is particularly important with respect to the real part, where the maximum is not found for small arguments but at values larger than zero. Hence, there is an implied frequency dependence of the optimum location of neighbouring superstructures with respect to the in- or anti-phase cross-coupling between moment components.

The interaction between propagation and spatial interface dependence is further illustrated in Figure 12, in which case the size of the response interface is doubled compared

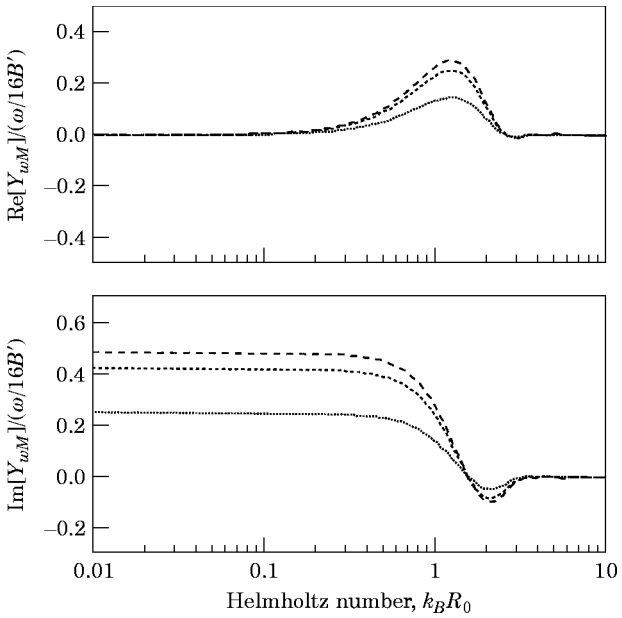

Figure 9. Normalized real (top) and imaginary (bottom) parts of moment cross-transfer mobility. $R_r/R_0 = 1$, $r_d/R_0 = 2$. ·····, $\varphi_d = \pi/12$; - - - -, $\varphi_d = \pi/6$; — —, $\varphi_d = \pi/4$.

with that of the excitation. Although the maxima of both real and imaginary parts are decreased slightly (compare Figure 11) the primary influence, however, is noted in the range of large Helmholtz numbers where both parts of the mobility are smoothed.

Finally, the cross-transfer mobility from moment to translatory velocity is presented in Figures 13–16 for some values of the interface radii and separations. Again, the angular

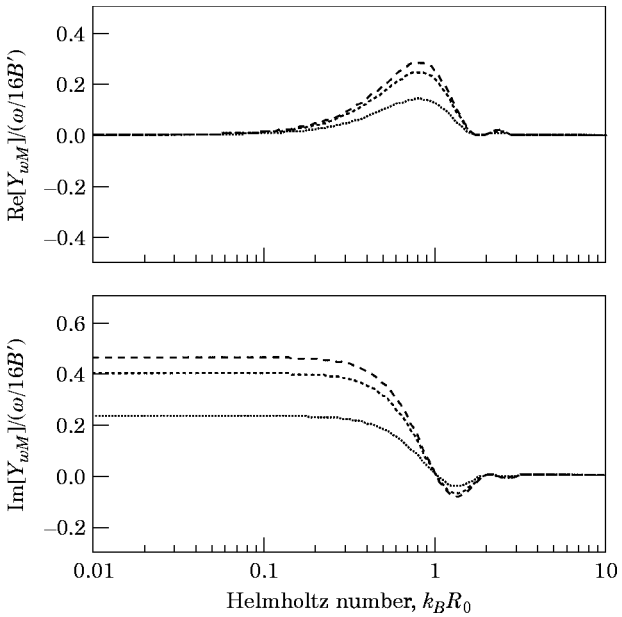

Figure 10. Normalized real (top) and imaginary (bottom) parts of moment cross-transfer mobility. $R_r/R_0 = 2$, $r_d/R_0 = 3$. ·····, $\varphi_d = \pi/12$; - - - -, $\varphi_d = \pi/6$; — —, $\varphi_d = \pi/4$.

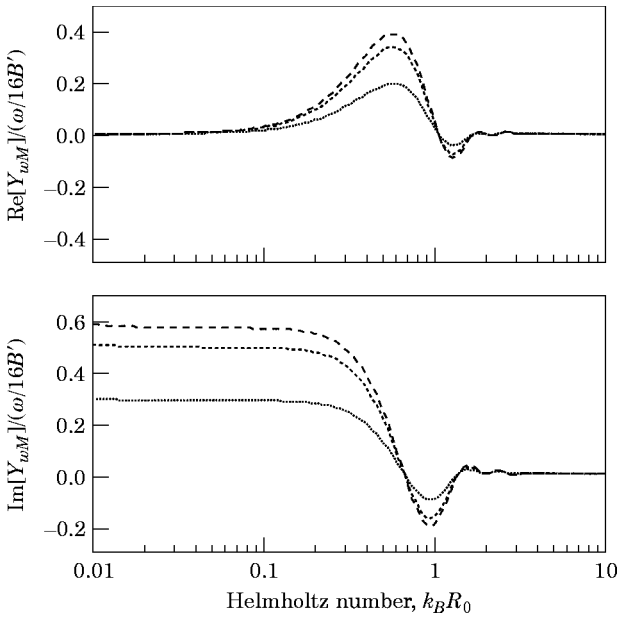

Figure 11. Normalized real (top) and imaginary (bottom) parts of moment cross-transfer mobility. $R_r/R_0 = 1$, $r_d/R_0 = 5$. ·····, $\varphi_d = \pi/12$; - - - -, $\varphi_d = \pi/6$; — —, $\varphi_d = \pi/4$.

position constitutes the parameter in the graphs. For adjacent interfaces, it is observed that in this case as well, the maximum of the real part of the cross-transfer mobility is obtained in the transition region where the imaginary part changes sign and turns from stiffness to mass controlled behaviour. Also, the imaginary part is a maximum in the transition region. As expected from the theoretical results for the nearfield range, the cross-transfer mobility

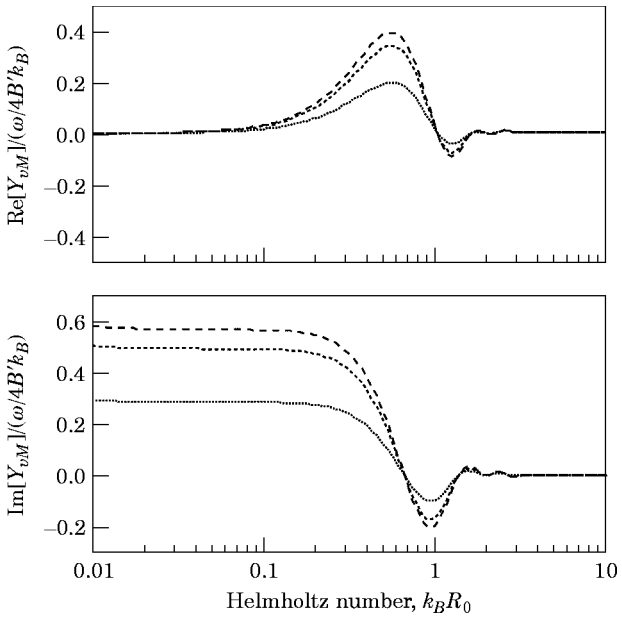

Figure 12. Normalized real (top) and imaginary (bottom) parts of moment cross-transfer mobility. $R_r/R_0 = 2$, $r_d/R_0 = 5$. ·····, $\varphi_d = \pi/12$; - - - -, $\varphi_d = \pi/6$; — —, $\varphi_d = \pi/4$.

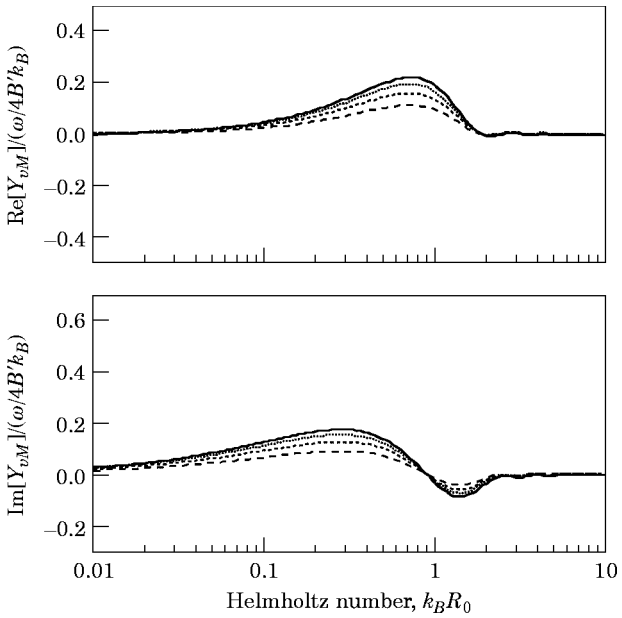

Figure 13. Normalized real (top) and imaginary (bottom) parts of moment translatory velocity cross-transfer mobility. $R_r/R_0 = 1$, $r_d/R_0 = 2$. ——, $\varphi_d = 0$; ·····, $\varphi_d = \pi/6$; - - - -, $\varphi_d = \pi/4$; — —, $\varphi_d = \pi/3$.

decreases with decreasing angle between the moment vector and the direction to the centre of the response interface (increasing φ_d). Reciprocally, an increase in the angle between a translatory force-excited interface and the rotational velocity vector component increases the cross-transfer mobility. Naturally, the alternating sign for large Helmholtz numbers reverses this pattern.

For interfaces close to each other, an increase of the size of the response interface leads to a slight decrease in the cross-transfer mobility as observed from a comparison of Figures 13 and 14. Moreover, the maxima of both parts and the onset of the sign alternation is shifted downwards in Helmholtz numbers.

The effect of interface separation (compare Figures 13 and 15 or Figures 14 and 16) is similar to that found for the cross-transfer mobility from moment to a rotational velocity component perpendicular to the moment vector, although not as pronounced. In this case, the maximum of the real part is governed by the first maximum of the first order Bessel function, implying that this maximum occurs at smaller Helmholtz numbers than that of the moment to rotational velocity cross-transfer mobility. Owing to the bending wave nearfield, the region in which the imaginary part is largest is generally found below that containing the maximum of the real part. Also, it should be borne in mind that a maximum in the propagation function is "filtered" by the interface geometries, so that its location in Helmholtz number space cannot be predicted exactly without considering all ingredients involved. Nevertheless, the presence of pronounced maxima in the cross-transfer mobilities demonstrates the necessity to take the spatial configuration into account for designs comprising multiple interfaces. Hereby, the difference in angular dependence between cross-transfer mobility from moment to a rotational velocity component perpendicular to the moment vector and cross-transfer mobility between rotational and translational field variables should be noted. While the former is a maximum for 45°, the latter peaks for 0°. Evidently, this difference establishes another set of design criteria which can be properly taken into account only when the characteristics of the source are available.

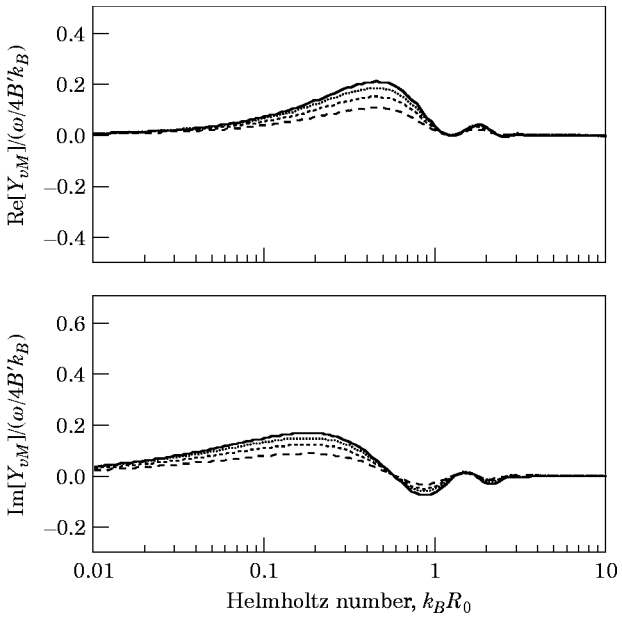

Figure 14. Normalized real (top) and imaginary (bottom) parts of moment translatory velocity cross-transfer mobility. $R_r/R_0 = 2$, $r_d/R_0 = 3$. ——, $\varphi_d = 0$; ·····, $\varphi_d = \pi/6$; - - - -, $\varphi_d = \pi/4$; — —, $\varphi_d = \pi/3$.

For sources involving rotating parts, the angular dependence of moment to translatory velocity cross-transfer coupling can be of substantial importance, because of the simultaneous dependence on the separation between excitation and response interfaces. As is illustrated by Figure 15, however, the alteration in sign in the mobility realizes a

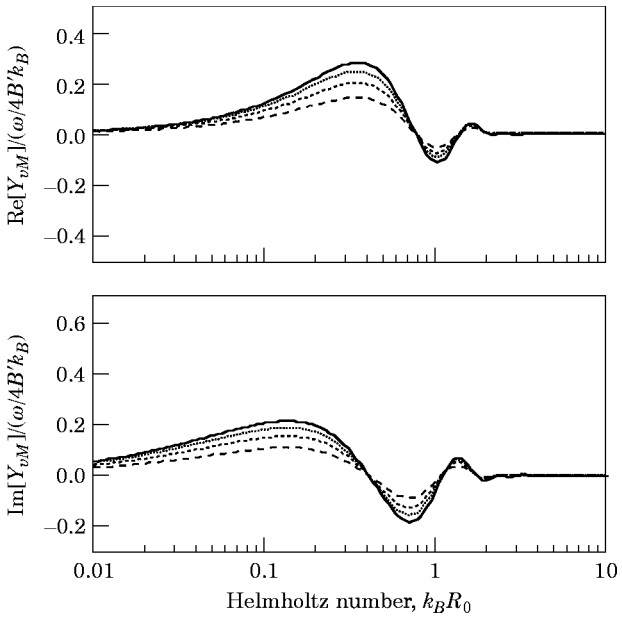

Figure 15. Normalized real (top) and imaginary (bottom) parts of moment to translatory velocity cross-transfer mobility. $R_r/R_0 = 1$, $r_d/R_0 = 5$. ——, $\varphi_d = 0$; ·····, $\varphi_d = \pi/6$; - - - -, $\varphi_d = \pi/4$; — —, $\varphi_d = \pi/3$.

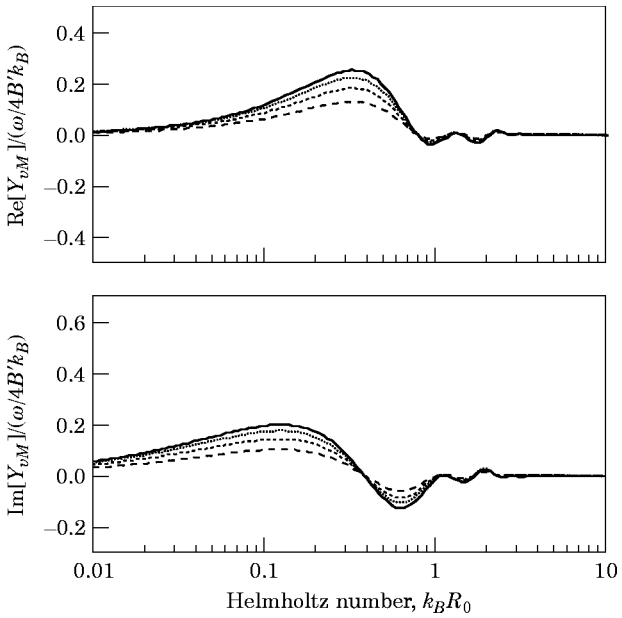

Figure 16. Normalized real (top) and imaginary (bottom) parts of moment to translatory velocity cross-transfer mobility. $R_r/R_0 = 2$, $r_d/R_0 = 5$. ——, $\varphi_d = 0$; ·····, $\varphi_d = \pi/6$; - - - -, $\varphi_d = \pi/4$; — —, $\varphi_d = \pi/3$.

possibility to suppress the influence of cross-coupling. Although the efficiency of tuning measures should not be overestimated, its potential for tonal excitation is worth consideration in conjunction with optimization of multiple interface configurations.

From a comparison of the results in Figures 15 and 16 one may again observe the smoothing effect of an increase of the dimensions of the response interface when removed from that of the excitation as discussed in conjunction with the results presented in Figures 11 and 12. In an absolute sense, the moment to translatory velocity cross-transfer mobility increases linearly with frequency for small Helmholtz numbers and decreases with frequency raised to the 3/4 power in the "farfield" behaviour range, which reinforces an overall maximum in the transition region. The frequency dependence in the upper range is identical for all elements and accordingly the influence of transfer and cross-transfer elements vanishes in the limit. In comparison with ordinary point excitation, however, the distributed excitation and response act to enhance the attenuation.

In contrast to the transfer mobility components, the cross-transfer mobilities all are simple functions of the angle between the excitation component and the centre of the response interface. This means that the angular and distance effects as well as that of interface geometry are separable and can be optimized independently.

It is clear from the numerical examples presented that the important range is below and at the transition from near to farfield behaviour. This does not mean that the mobilities are necessarily negligible in the farfield range but, rather, demonstrates that the transfer and cross-transfer contributions are far from subordinate.

4. CONCLUDING REMARKS

The theoretical conclusion that, for closed contour interfaces between superstructures and recipients, the zero and first order excitation distributions constitute the prime

components in structure-borne sound and vibration transmission, substantially facilitates the treatment of subsystem assemblies with extended interfaces. In turn, the interface mobilities proposed herein establish fundamental subsystem characteristics for a reformulation of the transmission across large interfaces, into an approach identical to that for point-like contact.

The complex mobilities derived for the directly excited interface, under the assumption of annular shape, clearly demonstrate that for Helmholtz numbers $k_B R$ smaller than unity where R is the radius of the interface, the ordinary point mobility concept is valid. For the transfer and cross-transfer mobilities, however, two interface geometries are involved, and it is found that the Helmholtz numbers for both should be less than unity to employ the corresponding point quantities. In general therefore, a criterion for an assessment of the applicability of "point" quantities results from the perimeter of the interfaces being less than the wavelength of the governing wave. For Helmholtz numbers larger than unity, the spatial matching of the excitation distribution and the trace of the free waves in the excited structure govern the signatures of the mobilities.

The geometry assumed in the analysis, i.e., annular, continuous interfaces between super- and substructures, quantitatively restricts the application of the mobilities derived to this shape. In a qualitative sense, however, the results are applicable and valid since all geometrical aspects are taken into account and, for not too extreme shapes of the interfaces, the results presented herein should establish satisfactory approximations, provided that the perimeter of the hollow cross-section is preserved. This means that the mobilities derived also provide insight into the implications of interfaces made up by groups of contact points. Moreover, in this study mobilities are derived for a thin, infinite plate, partly owing to the theoretical transparency but primarily because of the practical significance of such structures in noise and vibration control. It can thus be concluded that for thin, plate-like structures, all interface mobility elements decrease with frequency for large Helmholtz numbers provided that the net force or moment remains invariant. Physically, this can be interpreted as an overall, increasing spatial mismatch in trace wavelength at the interfaces and the low Helmholtz number range, accordingly, becomes the more significant. For transfer and cross-transfer interface mobilities, on the other hand, the emphasis is either on the region of small Helmholtz numbers where transfer mobilities are generally large or on the transition region in the case of cross-transfer mobilities. It is hence reasonable to consider particularly the low and mid-frequency ranges at a design stage.

It is found that the asymptotes developed for direct interface mobilities are applicable for all of the Helmholtz number ranges below and above unity respectively. In the immediate vicinity of unity, the asymptotes regarding the real parts are conservative, while those for the imaginary parts yield slight underestimates. Owing to the progressing spatial mismatch for large Helmholtz numbers, one can conclude that ordinary "point" quantities always constitute a conservative estimate. Furthermore, as in the case of ordinary point excitation, the real part of the interface force mobility is essentially resistive in nature. In contrast, however, a small reactive part results when the excitation is distributed over an annular interface. The real part of the moment mobility has a global maximum for Helmholtz numbers just below two and the imaginary part is stiffness controlled in virtually all of the range.

From the asymptotes related to the interface transfer and cross-transfer mobilities for small Helmholtz numbers, it is established that there are direct dependencies on the geometries of the interfaces as well as their relative locations. The applicability of the pertinent asymptotic expressions developed, therefore, varies with the relative parameter

magnitude. This means that for multiple interfaces, an eventually important aspect of design is the spatial orientation and optimization. The numerical results also indicate that inequality of the dimensions of excitation and response interfaces leads to a strengthened influence at low frequencies. For large Helmholtz numbers, the signature is that of a damped oscillation where, in addition to frequency, the decay is dependent on the dimensions of the interfaces as well as the distance. Hence, with respect to the transfer and cross-transfer characteristics, ordinary point quantities do not necessarily realize upper bounds. Although herein only the zero and first order excitation distributions are considered explicitly, the analysis is straightforwardly generalizable to higher order distributions when required. It is to be noted, however, that such an extension also implies a growing number of interface cross-transfer mobility elements.

It should be emphasized that although the results presented above are quantitatively valid only for thin plates and hence, in some cases in practice, there may be limitations introduced by the fact that the governing wavelength of the recipient becomes comparable with the recipient thickness and a continuum theoretical formulation should be employed [3], the spatial and configurative dependencies discussed remain valid. Moreover, for Helmholtz numbers below unity, the rigid indenter contact condition corresponds to an annular excitation [7] and thus the analyses presented above are also valuable for non-hollow superstructures provided that its rigidity is large compared with that of the recipient. By virtue of the superposition principle, the approach presented is readily extended to handle arbitrary excitation fields over wide annular and circular contact areas from integration in the radial direction.

Finally, the interface mobility elements for plate-like structures are directly implementable in design procedures for multiple, single unit, superstructures. For built-up, multi-unit superstructures such as extended and partitioned machinery seatings, the results can be superposed to give insight into the performance and characteristics of the recipient. Under the assumption of predominant global behaviour of superstructures, this approach establishes a possibility to work with a conventional transmission line formulation without recourse to an integral equation formulation.

ACKNOWLEDGMENT

The study has been financially supported by TNO Defence Research.

REFERENCES

1. B. A. T. Petersson 1994 *Journal of Sound and Vibration* **176**, 625–639. Efficiency of annularly distributed moment and force excitation regarding structural acoustic power transmission to plate-like structures.
2. A. S. Nikiforov 1974 *Soviet Physics—Acoustics* **19**, 372–374. Excitation of an infinite plate by a transverse force distributed around a circle.
3. B. A. T. Petersson and M. Heckl 1996 *Journal of Sound and Vibration* **196**, 295–321. Concentrated excitation of structures.
4. B. Petersson 1984 *Journal of Sound and Vibration* **94**, 495–524. The prerequisites for measuring mobility using annular transducer accessories.
5. L. Cremer and M. Heckl 1995 *Körperschall*. Berlin: Springer-Verlag.
6. B. Petersson 1986 *Journal of Sound and Vibration* **108**, 471–485. A thin-plate model for the moment mobility at T-intersections of plates.
7. B. A. T. Petersson and M. Heckl 1995 *Proceedings of the* 15*th International Congress on Acoustics*, *Trondheim*, 543–546. Local deformation revisited.
8. M. Abramowitz and I. A. Stegun 1972 *Handbook of Mathematical Functions*. New York: Dover.

APPENDIX I: INTERFACE FORCE TRANSFER MOBILITY

From equations (22) and (23), the spatially averaged force transfer mobility can be written as

$$\overline{Y_{vF}}(r_d, \varphi) = \frac{\omega}{8B'k_B^2}\frac{1}{2\pi}\left\{\mathrm{J}_0(k_BR_0)\left[\int_0^{2\pi}\mathrm{J}_0(k_B\sqrt{R_r^2 + r_d^2 - 2R_rr_d\cos\psi})\,\mathrm{d}\psi\right.\right.$$

$$\left. - \mathrm{i}\int_0^{2\pi}\mathrm{N}_0(k_B\sqrt{R_r^2 + r_d^2 - 2R_rr_d\cos\psi})\,\mathrm{d}\psi\right]$$

$$- \mathrm{i}\mathrm{I}_0(k_BR_0)\left[\int_0^{2\pi}\mathrm{J}_0(-\mathrm{i}k_B\sqrt{R_r^2 + r_d^2 - 2R_rr_d\cos\psi})\,\mathrm{d}\psi\right.$$

$$\left.\left. - \mathrm{i}\int_0^{2\pi}\mathrm{N}_0(-\mathrm{i}k_B\sqrt{R_r^2 + r_d^2 - 2R_rr_d\cos\psi})\,\mathrm{d}\psi\right]\right\}, \tag{AI.1}$$

in view of the relation

$$\mathrm{H}_0^{(2)}(-\mathrm{i}z) = (2\mathrm{i}/\pi)\mathrm{K}_0(z). \tag{AI.2}$$

Provided that $k_BR_r < k_Br_d$, which is always the case when the dimensions of the annular excitation interface are equal to or larger than those of the response interface and a transfer mobility is considered, then [6]

$$\int_0^{\pi}\mathrm{J}_0(\sqrt{\alpha^2 + \beta^2 - 2\alpha\beta\cos x})\,\mathrm{d}x = \sqrt{\pi}\Gamma(1/2)\mathrm{J}_0(\alpha)\mathrm{J}_0(\beta) \tag{AI.3}$$

and

$$\int_0^{\pi}\mathrm{N}_0(\sqrt{\alpha^2 + \beta^2 - 2\alpha\beta\cos x})\,\mathrm{d}x = \sqrt{\pi}\Gamma(1/2)\mathrm{J}_0(\alpha)\mathrm{N}_0(\beta), \tag{AI.4}$$

where α and β are identified as k_BR_r and k_Br_d respectively. Since J_0 and N_0 are even functions, the result presented in equation (25) follows.

Owing to the fact that the transfer mobility is symmetric with respect to k_BR_r and k_BR_0, one can infer that the condition of $k_BR_r < k_Br_d$ becomes irrelevant since, for a difference in interface dimension and the two interfaces being adjacent, one can always circumvent the troublesome configuration by consideration of the reciprocal case.

As a side result, the derivation given above establishes the solution of the integrals

$$\int_0^{\pi}\mathrm{K}_0(\sqrt{\alpha^2 + \beta^2 - 2\alpha\beta\cos x})\,\mathrm{d}x = -2\mathrm{i}\pi^2\mathrm{I}_0(\alpha)\mathrm{K}_0(\beta), \qquad |\alpha| < |\beta|, \tag{AI.5}$$

and

$$\int_0^{\pi}\mathrm{I}_0(\sqrt{\alpha^2 + \beta^2 - 2\alpha\beta\cos x})\,\mathrm{d}x = \pi\mathrm{I}_0(\alpha)\mathrm{I}_0(\beta). \tag{AI.6}$$

APPENDIX II: INTERFACE MOMENT TRANSFER MOBILITY

From equation (27) the effective moment transfer mobility with respect to the first order (rocking) excitation distribution can be rewritten as

$$\overline{Y_{vM,\parallel}}(r_d, \varphi_d) = \frac{\omega}{4B'k_B R_r}\Bigg[-\frac{\cos\varphi_d}{(k_B R_0)}\frac{1}{\pi}\int_{-\pi}^{\pi} \cos\psi \,\{\cos\varphi_d \cos\chi - \sin\varphi_d \sin\chi\}\Bigg\{\mathrm{J}_1(k_B R_0)\mathrm{H}_1^{(2)}(k_B r) - \mathrm{i}\frac{2}{\pi}\mathrm{I}_1(k_B R_0)\mathrm{K}_1(k_B r)\Bigg\}\,\mathrm{d}\psi + \frac{\sin\varphi_d}{(k_B R_0)}\frac{1}{\pi}\int_{-\pi}^{\pi} \sin\psi\{\cos\varphi_d\cos\chi - \sin\varphi_d\sin\chi\}\Bigg\{\mathrm{J}_1(k_B R_0)\mathrm{H}_1^{(2)}(k_B r) - \mathrm{i}\frac{2}{\pi}\mathrm{I}_1(k_B R_0)\mathrm{K}_1(k_B r)\Bigg\}\,\mathrm{d}\psi\Bigg]. \tag{AII.1}$$

Similarly, the cross-transfer mobility involving the rotational response with its unit vector perpendicular to that of the moment can be found to be formally given by

$$\overline{Y_{vM,\perp}}(r_d, \varphi_d) = -\frac{\omega}{4B'k_B R_r}\Bigg[-\frac{\sin\varphi_d}{(k_B R_0)}\frac{1}{\pi}\int_{-\pi}^{\pi} \cos\psi \,\{\cos\varphi_d \cos\chi - \sin\varphi_d \sin\chi\}\Bigg\{\mathrm{J}_1(k_B R_0)\mathrm{H}_1^{(2)}(k_B r) - \mathrm{i}\frac{2}{\pi}\mathrm{I}_1(k_B R_0)\mathrm{K}_1(k_B r)\Bigg\}\,\mathrm{d}\psi + \frac{\cos\varphi_d}{(k_B R_0)}\frac{1}{\pi}\int_{-\pi}^{\pi} \sin\psi\{\cos\varphi_d\cos\chi - \sin\varphi_d\sin\chi\}\Bigg\{\mathrm{J}_1(k_B R_0)\mathrm{H}_1^{(2)}(k_B r) - \mathrm{i}\frac{2}{\pi}\mathrm{I}_1(k_B R_0)\mathrm{K}_1(k_B r)\Bigg\}\,\mathrm{d}\psi\Bigg]. \tag{AII.2}$$

Let

$$S_{11} = \int_{-\pi}^{\pi} \cos\psi\,\cos\chi \mathrm{H}_1^{(2)}(k_B\sqrt{R_r^2 + r_d^2 - 2R_r r_d\cos\psi})\,\mathrm{d}\psi,$$

$$S_{12} = \int_{-\pi}^{\pi} \cos\psi\,\sin\chi \mathrm{H}_1^{(2)}(k_B\sqrt{R_r^2 + r_d^2 - 2R_r r_d\cos\psi})\,\mathrm{d}\psi,$$

$$S_{21} = \int_{-\pi}^{\pi} \cos\psi\,\cos\chi \mathrm{K}_1(k_B\sqrt{R_r^2 + r_d^2 - 2R_r r_d\cos\psi})\,\mathrm{d}\psi,$$

$$S_{22} = \int_{-\pi}^{\pi} \cos\psi\,\sin\chi \mathrm{K}_1(k_B\sqrt{R_r^2 + r_d^2 - 2R_r r_d\cos\psi})\,\mathrm{d}\psi, \tag{AII.3a–d}$$

and

$$S_{31} = \int_{-\pi}^{\pi} \sin\psi \cos\chi \mathrm{H}_1^{(2)}(k_B\sqrt{R_r^2 + r_d^2 - 2R_r r_d \cos\psi})\,\mathrm{d}\psi,$$

$$S_{32} = \int_{-\pi}^{\pi} \sin\psi \sin\chi \mathrm{H}_1^{(2)}(k_B\sqrt{R_r^2 + r_d^2 - 2R_r r_d \cos\psi})\,\mathrm{d}\psi,$$

$$S_{41} = \int_{-\pi}^{\pi} \sin\psi \cos\chi \mathrm{K}_1(k_B\sqrt{R_r^2 + r_d^2 - 2R_r r_d \cos\psi})\,\mathrm{d}\psi,$$

$$S_{42} = \int_{-\pi}^{\pi} \sin\psi \sin\chi \mathrm{K}_1(k_B\sqrt{R_r^2 + r_d^2 - 2R_r r_d \cos\psi})\,\mathrm{d}\psi, \qquad \text{(AII.4a–d)}$$

represent the integrals in equations (AII.1) and (AII.2). There are four principal kinds of which S_{11} is an example of the first and which can be rewritten by means of Graf's addition theorem (see, e.g. reference [6]) as

$$\begin{aligned} S_{11} &= \int_{-\pi}^{\pi} \cos\psi \sum_{q=-\infty}^{\infty} \mathrm{H}_{q+1}^{(2)}(k_B r_d)\mathrm{J}_q(k_B R_r)\cos q\psi\,\mathrm{d}\psi \\ &= \sum_{q=-\infty}^{\infty} \mathrm{H}_{q+1}^{(2)}(k_B r_d)\mathrm{J}_q(k_B R_r)\int_{-\pi}^{\pi} \cos\psi\cos q\psi\,\mathrm{d}\psi \\ &= \pi \mathrm{J}_1(k_B R_r)[\mathrm{H}_2^{(2)}(k_B r_d) - \mathrm{H}_0^{(2)}(k_B r_d)], \end{aligned} \qquad \text{(AII.5)}$$

owing to the fact that all multiple angle integrals are identically zero.

Indeed, this scheme is valid also for the modified Bessel functions, since

$$\mathrm{K}_n(z) = -(\pi\mathrm{i}/2)\mathrm{e}^{-n\pi\mathrm{i}/2}\mathrm{H}_n^{(2)}(-\mathrm{i}z), \qquad \text{(AII.6)}$$

from which the Bessel and Neumann functions can be regained so that S_{21} is found to be given by

$$\begin{aligned} S_{21} &= -\frac{\pi}{2}\int_{-\pi}^{\pi} \cos\psi\cos\chi \mathrm{H}_1^{(2)}(-\mathrm{i}k_B\sqrt{R_r^2 + r_d^2 - 2R_r r_d\cos\psi})\,\mathrm{d}\psi \\ &= -\frac{\pi}{2}\sum_{q=-\infty}^{\infty} \mathrm{H}_{q+1}^{(2)}(-\mathrm{i}k_B r_d)\mathrm{J}_q(-\mathrm{i}k_B R_r)\int_{-\pi}^{\pi} \cos\psi\cos q\psi\,\mathrm{d}\psi \\ &= -(\pi^2/2)\mathrm{J}_1(-\mathrm{i}k_B R_r)[\mathrm{H}_2^{(2)}(-\mathrm{i}k_B r_d) - \mathrm{H}_0^{(2)}(-\mathrm{i}k_B r_d)] \\ &= \pi \mathrm{I}_1(k_B R_r)[\mathrm{K}_2(k_B r_d) + \mathrm{K}_0(k_B r_d)]. \end{aligned} \qquad \text{(AII.7)}$$

The second and third kinds of integrals involve either

$$\int_{-\pi}^{\pi} \cos\psi \sin q\psi\,\mathrm{d}\psi \qquad \text{or} \qquad \int_{-\pi}^{\pi} \sin\psi\cos q\psi\,\mathrm{d}\psi, \qquad \text{(AII.8, AII.9)}$$

which both vanish owing to orthogonality. The fourth kind leads to

$$S_{32} = \int_{-\pi}^{\pi} \sin\psi \sum_{q=-\infty}^{\infty} \mathrm{H}^{(2)}_{q+1}(k_B r_d)\mathrm{J}_q(k_B R_r)\sin q\psi \,\mathrm{d}\psi$$

$$= \sum_{q=-\infty}^{\infty} \mathrm{H}^{(2)}_{q+1}(k_B r_d)\mathrm{J}_q(k_B R_r)\int_{-\pi}^{\pi} \sin\psi \sin q\psi \,\mathrm{d}\psi$$

$$= \pi \mathrm{J}_1(k_B R_r)[\mathrm{H}^{(2)}_0(k_B r_d) + \mathrm{H}^{(2)}_2(k_B r_d)] \tag{AII.10}$$

as well as

$$S_{42} = -\frac{\pi}{2}\int_{-\pi}^{\pi} \sin\psi \sin\chi \mathrm{H}^{(2)}_1(-\mathrm{i}k_B\sqrt{R_r^2 + r_d^2 - 2R_r r_d\cos\psi})\,\mathrm{d}\psi$$

$$= -\frac{\pi}{2}\sum_{q=-\infty}^{\infty} \mathrm{H}^{(2)}_{q+1}(-\mathrm{i}k_B r_d)\mathrm{J}_q(-\mathrm{i}k_B R_r)\int_{-\pi}^{\pi} \sin\psi \sin q\psi \,\mathrm{d}\psi$$

$$= -(\pi^2/2)\mathrm{J}_1(-\mathrm{i}k_B R_r)[\mathrm{H}^{(2)}_2(-\mathrm{i}k_B r_d) + \mathrm{H}^{(2)}_0(-\mathrm{i}k_B r_d)]$$

$$= \pi \mathrm{I}_1(k_B R_r)[\mathrm{K}_2(k_B r_d) - \mathrm{K}_0(k_B r_d)], \tag{AII.11}$$

and, as could be expected, these are identical to those of the first kind. Hence, substitution back into equations (AII.1) and (AII.2) yields the effective interface moment transfer mobilities as stated in equations (28).

APPENDIX III: SYMBOLS AND NOTATION

A	function
B'	flexural stiffness per unit length
E	Young's modulus, amplitude
F	force
H	Hankel function
I	modified Bessel function
J	Bessel function
K	modified Bessel function
L	differential operator
M	moment
N	natural number
N	Newmann function
R	radius of interface
S	integral, area
Y	mobility
a, b	auxiliary variables
i	imaginary unit
k	wavenumber
q	number
r	polar co-ordinate
v	translational velocity
w	rotational velocity
z	complex variable
γ_E	Euler's constant
δ	Dirac's delta function
χ	auxiliary angle
ψ	auxiliary angle
ζ	complex variable
φ	polar co-ordinate
ρ	density
ω	angular frequency
σ	normal stress

Indices

B	flexural
F	force
M	moment
n	order
v	translational velocity
w	rotational velocity
q	index, order
d	interface centre
r	response interface
0	excitation interface

Notation

$\cdot\cdot$	time differentiation twice
*	complex conjugate
$\wedge$	wavenumber spectral quantity
$\parallel$	parallel
$\perp$	perpendicular
$\bar{}$	spatial average